Cell Reports

Report

Force-induced motions of the PIEZO1 blade probed with fluorimetry

Graphical abstract

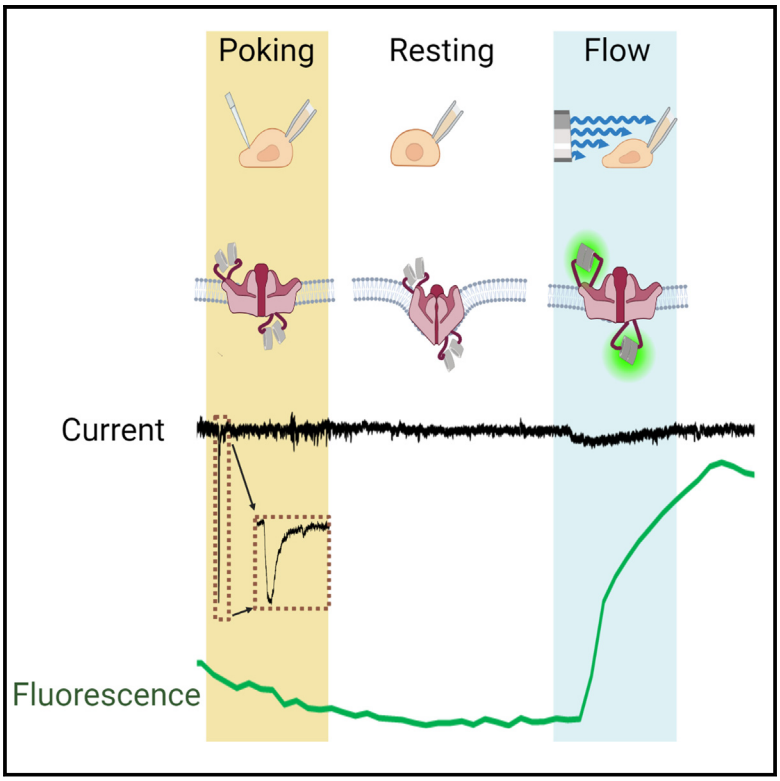

Highlights

- Optical probes track PIEZO1 conformational changes at two distant blade positions
- Two independent probes respond to flow, not indentations or osmotic swelling
- Fluorescence signals from both probes correlate with flow-induced channel opening
- Both probes respond to fluid shear stress stimuli of low, but not high, intensity

Authors

Alper D. Ozkan, Tharaka D. Wijerathne, Tina Gettas, Jérôme J. Lacroix

Correspondence

jlacroix@westernu.edu

In brief

Ozkan et al. use conformation-sensitive fluorescent probes to track force-induced rearrangements of PIEZO1's mechanosensory blade domains. Two probes inserted far apart in the blade independently "light up" as channels activate in response to low-intensity fluid shear stress but not to other tested mechanical stimuli.

Ozkan et al., 2023, Cell Reports *42*, 112837
August 29, 2023
https://doi.org/10.1016/j.celrep.2023.112837

CellPress

Cell Reports

CellPress
OPEN ACCESS

Report

Force-induced motions of the PIEZO1 blade probed with fluorimetry

Alper D. Ozkan,[1,3] Tharaka D. Wijerathne,[2,3] Tina Gettas,[2] and Jérôme J. Lacroix[2,4,*]
[1]Department of Pharmaceutical Microbiology, Bahçeşehir University, Yıldız, Çırağan Cd, 34349 Beşiktaş/İstanbul, Turkey
[2]Department of Basic Medical Sciences, Western University of Health Sciences, 309 E. Second St, Pomona, CA 91766, USA
[3]These authors contributed equally
[4]Lead contact
*Correspondence: jlacroix@westernu.edu
https://doi.org/10.1016/j.celrep.2023.112837

SUMMARY

Mechanical forces are thought to activate mechanosensitive PIEZO channels by changing the conformation of a large transmembrane blade domain. Yet, whether different stimuli induce identical conformational changes in this domain remains unclear. Here, we repurpose a cyclic permuted green fluorescent protein as a conformation-sensitive probe to track local rearrangements along the PIEZO1 blade. Two independent probes, one inserted in an extracellular site distal to the pore and the other in a distant intracellular proximal position, elicit sizable fluorescence signals when the tagged channels activate in response to fluid shear stress of low intensity. Neither cellular indentations nor osmotic swelling of the cell elicit detectable fluorescence signals from either probe, despite the ability of these stimuli to activate the tagged channels. High-intensity flow stimuli are ineffective at eliciting fluorescence signals from either probe. Together, these findings suggest that low-intensity fluid shear stress causes a distinct form of mechanical stress to the cell.

INTRODUCTION

Mechanosensitive PIEZO channels couple mechanical forces to intracellular signaling, enabling organisms to control tissue growth, regulate the flow and pressure of internal fluids, and map the topography of their environment.[1] PIEZO1, one of only two vertebrate PIEZO members,[2,3] responds to diverse mechanical stimuli, including stretch,[4–6] hydrostatic pressure,[7] fluid shear stress,[8–13] intracellular traction forces,[14] hypotonic shocks,[6,15,16] nanoscale substrate displacements,[17] mechanical indentations,[2] and low-intensity ultrasound.[18,19] This broad mechanical sensitivity mirrors the breadth of physiological functions governed by PIEZO1 across cells, organs, and physiological systems.[9,11,12,20–30]

PIEZO1 possesses a homotrimeric structure encompassing a central pore region and three non-coplanar transmembrane blade domains, conferring the channel a unique bowl shape.[31–35] Physical manipulations of the PIEZO1 blade alter channel sensitivity to mechanical forces,[36–39] suggesting that this domain senses mechanical stimuli by changing its conformation. For instance, high-speed atomic microscopy kymographs reveal that the PIEZO1 blades reversibly flatten under compression, while cryoelectron microscopy images of PIEZO1 reconstituted in proteoliposomes show that the curvature of its blades changes as a function of the vesicle's intrinsic curvature.[40,41] Molecular dynamics simulations reveal that stretching[42] or flattening[43] the lipid bilayer causes PIEZO1 to flatten its blades and open its pore.

Yet, in spite of these efforts, direct experimental evidence for the coupling between PIEZO1 blade motions and pore opening remains scarce. Indeed, although a recent structure captures a flattened channel, this structure has a low resolution in the pore, making it difficult to link this conformation to a functional state.[41] In addition, although crosslinking the blade to an extracellular cap domain above the pore abolishes mechanically induced currents, this loss of function could be caused by a lack of mobility in the cap, not in the blade.[37] Furthermore, although actuation of the blade with magnetic nanoparticles modulates current kinetics, it fails to alter open probability in the absence of a mechanical stimulus.[38] Lastly, although genetic deletion of the blade abolishes mechanosensitivity,[36] claims that transplanting this domain confers mechanosensitivity to a naive trimeric channel have been disputed.[44,45]

Whether or not opening of the pore is caused by conformational changes in the blade, it remains unclear whether different mechanical stimuli cause similar conformational rearrangements. To address these questions, here we track force-induced rearrangements of the PIEZO1 blades *in cellulo* using site-specific fluorimetry, enabled by the exquisite sensitivity of fluorescent probes to local protein motions.

RESULTS

Generation of PIEZO1-cpGFP constructs

Site-specific fluorimetry, the detection of changes in fluorescence emission from chromophores attached to specific protein sites, enables tracking conformational changes in voltage-gated and ligand-gated ion channels.[46,47] Here, we adapt this technique to PIEZO1 using cyclic permuted green fluorescent

proteins (cpGFPs) as tractable conformation-sensitive probes. Indeed, conformational changes in the host protein backbone near the site of cpGFP insertion often lead to a reduction (quenching) or increase (dequenching) of cpGFP fluorescence emission through chemical changes in the chromophore vicinity.[48] Although the degree of cpGFP fluorescence modulation is generally not quantitatively related to the physical displacement of the host protein backbone, these fluorescence changes enable tracking local conformational changes, a property that has sparked the development of numerous genetically encodable fluorescent indicators.[49–54]

We cloned cpGFP from the voltage-indicator ASAP1[55] and inserted it at the carboxyl end of mouse PIEZO1 (mPIEZO1) residues 86, 300, and 1591 (Table S1). These positions are known to tolerate proteinogenic modifications with no major functional impacts[4,15,38] and are spread along the PIEZO blade (Figure S1A). We also inserted cpGFP at residue 656, i.e., adjacent to an extracellular loop necessary for mechanical activation,[35] and at residue 1299, i.e., at the distal end of a long intracellular beam anticipated to transmit force from the blade to the pore.[35,39]

We first tested whether the presence of the cpGFP at these positions impacts channel function by measuring the sensitivity of our constructs to the chemical agonist Yoda1.[56] Mechanoinsensitive HEK293T$^{\Delta PZ1}$ cells, in which expression of endogenous human PIEZO1 is abolished,[57] were cotransfected with a plasmid encoding one of our constructs (named 86, 300, 656, 1299, and 1591) and a plasmid encoding the red calcium indicator jRGECO1a to avoid spectral overlap with cpGFP.[58] We next monitored jRGECO1a fluorescence before and after acute application of Yoda1. In calcium imaging assays, the saturating Yoda1 concentration varies across the literature, from ~10 to ~100 μM,[15,56,59,60] perhaps due to differences in sensitivity/saturability of calcium reporters. In electrophysiology assays, the effects of Yoda1 on PIEZO1 kinetics do not appear to saturate at the maximal tested concentration of 30 μM.[61] In our calcium imaging assay, we chose a conservative concentration of 100 μM to maximize the effects of Yoda1, enabling even faint channel activity from our constructs to be captured. During the time course of calcium imaging, the maximal fluorescence change, or m$\Delta F/F_0$, induced by Yoda1 was, on average, clearly not different between cells transfected with 656 or 1299 and cells transfected with jRGECO1 alone (Kruskal-Wallis p values with Dunn's multiple comparisons correction > 0.999) (Figure S1B), suggesting that these two constructs are functionally impaired. In contrast, the m$\Delta F/F_0$ values tend to be higher than the negative control in cells transfected with wild-type (WT) or with 86, 300, or 1591. We thus focus on these three constructs.

cpGFP probes are insensitive to cellular indentations

We next used whole-cell poking electrophysiology to show that mechanical indentations of the cell with a blunt glass probe (0–10 μm displacement) elicit ionic currents in 86, 300, and 1591 but not in cells transfected with Lck-cpGFP, a mechanoinsensitive construct in which cpGFP is fused to the membrane-bound N-terminal domain of the Lck kinase[49] (Figure 1A). Because macroscopic PIEZO1 currents rapidly inactivate,[3] we used the relative peak of mechanically induced currents (I/Imax) as a proxy for channel mechanosensitivity. Plotting I/Imax as a function of indentation depth produces sigmoid-like curves with similar mid-point activation depth (calculated using Boltzmann fitting; see STAR Methods) for WT mPIEZO1 (4.68 ± 0.14 μm), 86 (4.93 ± 0.09 μm), 300 (4.66 ± 0.16 μm), and 1591 (4.50 ± 0.08 μm) (Figure 1B). Although 300 is mechanosensitive, it yields smaller peak currents and current density (pA/pF; Figure 1C) relative to other constructs, mirroring its weaker sensitivity to Yoda1 (Figure S1B). Inactivation kinetics of poke currents (7 μm indentation) in 86, 1591, and 300 were not different from those measured in WT mPIEZO1 ($p > 0.3748$) (Figure 1D).

We next tested whether our probes fluorometrically respond to a 7 μm poke maintained for 1,500 ms. This poke stimulus tends to evoke larger calcium signals in cells cotransfected with jRGECO1a and WT mPIEZO1, 86, 300, or 1591 compared with control cells transfected with jRGECO1a alone ($0.0015 < p < 0.1030$) (Figures 1E and 1F). The same stimulus, however, did not seem to induce significant changes in cpGFP fluorescence in any tested transfection condition ($p > 0.3562$) (Figures 1G and 1H). Although small changes in fluorescence (m$\Delta F/F_0 < \pm 10\%$) occasionally occur during indentation of these cells, a careful visual examination of imaging data suggests that these changes are primarily due to unpreventable movements of the cell membrane during indentation rather than genuine changes of cpGFP fluorescence (Videos S1, S2, and S3). Narrower or deeper indentations were still ineffective at evoking fluorimetric cpGFP responses (data not shown).

cpGFP probes are insensitive to osmotic swelling

Next, we used pressure-clamp electrophysiology to show that cells transfected with 86, 300, and 1591, but not Lck-cpGFP, produce stretch-dependent currents that saturate and exhibit mid-point activation pressure (86: 45.43 ± 1.83 mmHg, 300: 40.37 ± 1.86 mmHg, and 1591: 49.22 ± 3.10 mmHg) comparable to that of cells transfected with WT mPIEZO1 (37.05 ± 1.05 mmHg) (Figures 2A and 2B). Consistent with previous observations, 300 yields smaller peak currents compared with the other constructs or WT mPIEZO1 (Figure 2C). Inactivation kinetics of stretch-activated currents in 86, 1591, and 300 currents (measured at −80 mmHg pipette pressure) were similar to those measured in WT mPIEZO1 (Kruskal-Wallis p values with Dunn's multiple comparisons correction > 0.7238) (Figure 2D).

To test whether our constructs are fluorimetrically sensitive to membrane stretch, we used acute hypotonic shock (~58 mOsmol L^{-1}). This stimulus slowly swells the cell over tens of seconds, stretching a large fraction of its membrane. This osmotic stimulus is more effective to visualize cpGFP fluorescence than pipette pressurization because the latter only stretches the minuscule membrane area captured by the patch pipette. Our osmotic stimulus evokes robust and transient calcium signals in cells cotransfected with jRGECO1a and with WT mPIEZO1, 86, 300, or 1591 compared with cells transfected with jRGECO1a alone ($0.0004 < p < 0.0254$) (Figures 2E and 2F). Like indentations, osmotic swelling was ineffective at eliciting detectable cpGFP fluorescence changes in 86, 300, or 1591, as cpGFP fluorescence emission in these constructs tends to monotonically decay before and during hypotonic stimulation,

CellPress
OPEN ACCESS

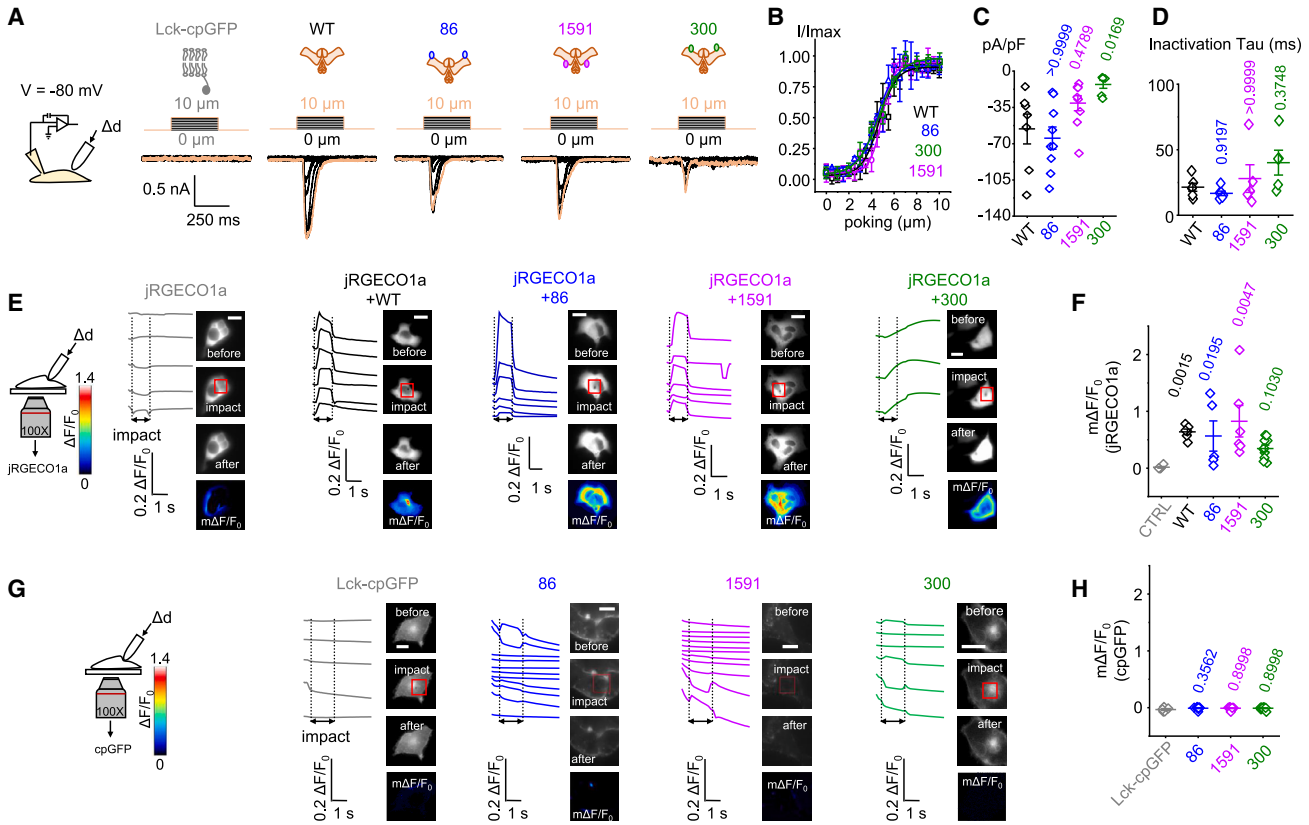

Figure 1. 86, 1591, and 300 are fluorimetrically silent to indentations

(A) Representative macroscopic current traces from cells transfected with Lck-cpGFP, WT mPIEZO1, 86, 1591, and 300 in response to poke stimuli.

(B) Relative peak current amplitude (I/Imax) plotted as a function of poking displacement (WT: n = 5; 86: n = 4; 300: n = 6; 1591: n = 6).

(C) Current density (pA/pF) from data shown in (A).

(D) Inactivation time constants of currents evoked by a 7 μm poke stimulus.

(E) Representative calcium-sensitive epifluorescence images and time course from cells transfected with a jRGECO1a plasmid and cotransfected or not (control) with WT mPIEZO1, 86, 1591, or 300 and stimulated with a 7 μm/1,500 ms poke stimulus (red squares).

(F) Scatter interval plots showing $m\Delta F/F_0$ values from experiments shown in (E).

(G) Representative cpGFP epifluorescence images and time course from cells expressing Lck-cpGFP, 86, 1591, and 300, stimulated with a 7 μm poke stimulus (red squares).

(H) Scatterplots showing cpGFP $m\Delta F/F_0$ values from experiments shown in (G).

In (E) and (G), scale bars represent 10 μm. Each point in (C), (D), (F), and (H) represents data from independent experiments, and numbers above plots indicate p values from Kruskal-Wallis tests with Dunn's multiple comparisons between each condition vs. WT (C and D), CTRL (F), or vs. Lck-cpGFP (H). Error bars: SEM. See also Figure S1 and Videos S1, S2, and S3.

likely due to photobleaching effects (Figures 2G and 2H). The lack of cpGFP response occurs despite osmotic swelling of the cells, which is clearly noticeable from visual examination of imaging data (Videos S4, S5, and S6).

cpGFP probes 86 and 1591 sense flow

We next seeded transfected cells into laminar flow chambers to test the sensitivity of our constructs to fluid shear stress, delivered by perfusing the chamber with Hank's balanced salt solution (HBSS) at a calibrated flow rate (see STAR Methods). A series of intermittent flow pulses (10 s on/10 s off) of small, incrementally increasing amplitudes (0.02–0.69 Pa) elicit robust and transient increase of cpGFP fluorescence emission (dequenching) in cells expressing 86 and 1591 but not 300 (Figure 3A; Videos S7 and S8). We previously showed that the same flow protocol fails to elicit fluorescence signals in cells transfected with Lck-cpGFP or with ASAP1, a voltage-sensitive membrane protein carrying a cpGFP at an extracellular position.[49,55] As expected, cells expressing Lck-cpGFP do not exhibit large cpGFP signals as seen in cells transfected with 86 or 1591 (Figure 3A). The fact that Lck-cpGFP and ASAP1 are insensitive to our flow protocol indicates that the signals emitted by 86 and 1591 depend on the presence of PIEZO1 acting as the host protein for cpGFP. This means that these signals are unlikely to be caused independently of conformational changes in PIEZO1, for example as a result of intermolecular collisions between cpGFP and surrounding lipid or solute molecules.

Next, we stimulated transfected cells using individual flow pulses of 10 s duration and 0.28 Pa amplitude. This low-intensity flow stimulus produces fluorescence signals whose time course

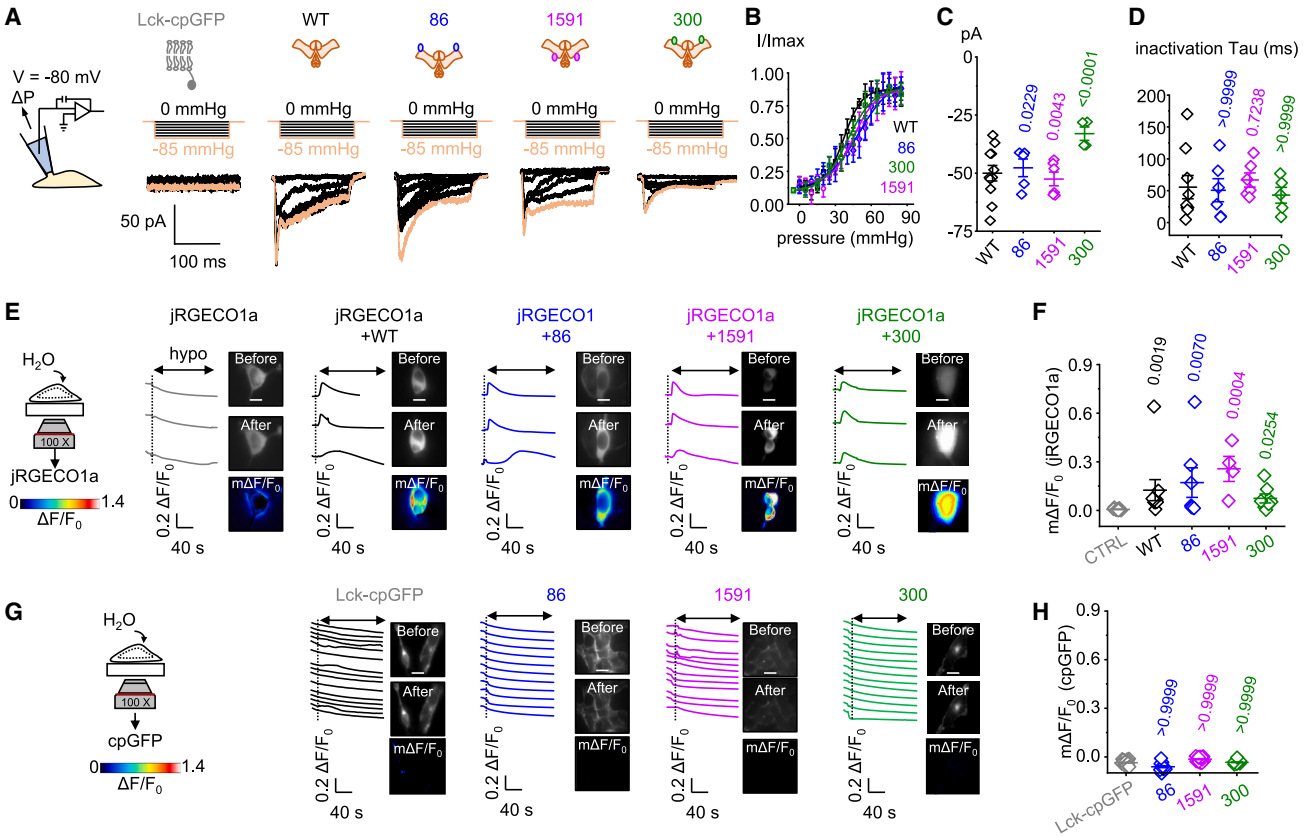

Figure 2. 86, 1591, and 300 are fluorimetrically silent to hypotonic shocks

(A) Representative pressure-induced macroscopic current traces from cells transfected with Lck-cpGFP, WT mPIEZO1, 86, 1591, and 300 (pressure pulses: from +5 to −85 mmHg).

(B) Relative peak current amplitude (I/Imax) plotted as a function of patch pressure (WT: n = 8; 86: n = 6; 300: n = 5; 1591: n = 5).

(C) Scatterplot comparing peak currents from data shown in (A) and (B).

(D) Inactivation time constants of currents evoked by −80 mmHg pressure.

(E) Representative jRGECO1a fluorescence images and time traces from cells transfected with a jRGECO1a plasmid only (CTRL) or cotransfected with Lck-cpGFP, mPIEZO1 WT, 86, 300, or 1591, and exposed to a hypotonic stress (~58 mOsmol L^{-1}).

(F) Scatter interval plots showing jRGECO1a $m\Delta F/F_0$ values from experiments described in (E).

(G) Representative cpGFP fluorescence images and time traces of 86, 1591, and 300 following exposure to a hypotonic solution.

(H) Scatter interval plots showing cpGFP $m\Delta F/F_0$ values from experiments described in (G).

In (E), and (G), scale bars represent 10 μm. Each dot in (C), (D), (F), and (H) represents a cell or a group of cells from independent experiments, and numbers above plots indicate p values from Kruskal-Wallis tests with Dunn's multiple comparisons against control. Error bars: SEM.

See also Videos S4, S5, and S6.

and amplitude vary from cell to cell (Figure 3B). The heterogeneity of the cpGFP signal may be explained by cell-to-cell variability in morphology, polarity, and adhesion profile, factors anticipated to affect the mechanical stress experienced by fluid shear stress.[62] Nevertheless, the mean maximal amplitude of these signals was not too different between 86 ($m\Delta F/F_0$ = 0.75 ± 0.11) and 1591 ($m\Delta F/F_0$ = 0.59 ± 0.17) (p = 0.0546) (Figure 3C). As observed using our multipulse protocol, no large cpGFP signals were detected in cells expressing 300, despite that fact that these cells exhibit baseline membrane green fluorescence, suggesting proper folding of the proteinogenic chromophore. The fact that not all cpGFP constructs respond to flow demonstrates that the property of cpGFP to elicit flow-induced fluorimetric signals strictly depends on its position within the PIEZO1 blade, as expected if these signals are produced by specialized rearrangements in this domain.

We next conducted calcium imaging experiments to test whether our low-intensity flow pulse (10 s/0.28 Pa) is sufficient to open the channel pore. Our data show that this flow pulse elicits larger calcium signals in cells cotransfected with jRGECO1a and WT mPIEZO1, 86, and 1591 compared with cells transfected with jRGECO1a only ($0.0277 < p < 0.0468$) (Figures 3D and 3E), showing that this standard flow stimulus is effective to activate these constructs. Although the same trend is observed for 300, the statistical significance is poor (p = 0.1896) as expected because cells transfected with 300 exhibit smaller responses to mechanical or chemical stimulations (Figures S1B, S1C, and S2C).

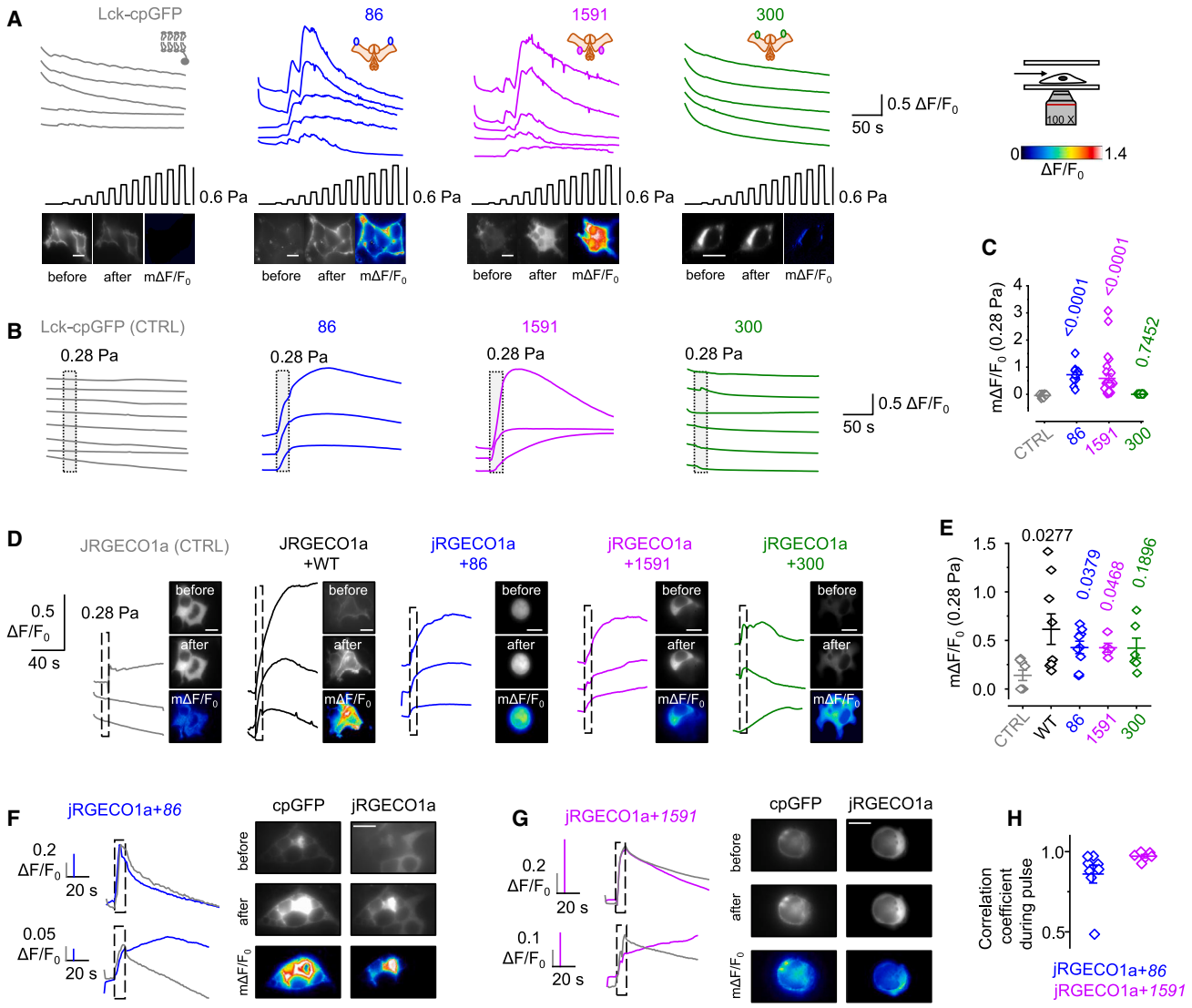

Figure 3. Flow stimuli induce robust fluorescent responses in both 86 and 1591

(A) Representative cpGFP fluorescence traces, static snapshots, and mΔF/F_0 images from cells expressing Lck-cpGFP 86, 1591, or 300, in response to shear stress applied in a series of 11 escalating flow pulses (duration: 10 s, magnitude: 0.022–0.691 Pa).

(B) Representative cpGFP fluorescence traces from cells expressing Lck-cpGFP 86, 1591, or 300 stimulated with a 10 s/0.28 Pa flow pulse.

(C) Scatterplot showing mΔF/F_0 values from experiments described in (B).

(D) Time course of jRGECO1a fluorescence from cells transfected with jRGECO1a and cotransfected or not (CTRL) with WT mPIEZO1, 86, 1591, or 300 and exposed to a 10 s/0.28 Pa flow pulse.

(E) Scatterplots showing jRGECO1a mΔF/F_0 values from experiments described in (D).

(F and G) Exemplar dual-fluorescence (jRGECO1a/cpGFP) time traces and images in cells transfected with 86 (F) or 1591 (G) and acutely stimulated with a 10 s/0.28 Pa flow pulse. Fluorescence time traces of 86, 1591, and jRGECO1a are shown in blue, purple, and gray, respectively.

(H) Scatterplots showing the value of Pearson's correlation coefficient during the duration of flow between cpGFP and jRGECO1a signals from experiments illustrated in (F) and (G).

In (A), (D), (F), and (G), scale bars represent 10 μm. Each dot in (C), (E), and (H) represents data from independent experiments. Numbers above plots in (C) and (E) indicate p values from Kruskal-Wallis tests with Dunn's multiple comparisons against control. Error bars: SEM.

See also Figure S2 and Videos S7 and S8.

Flow-induced cpGFP signals correlate with channel activation

We next used dual-wavelength imaging to simultaneously visualize flow-induced cpGFP and jRGECO1a signals in cells transfected with 86 or 1591. Our data show that both signals occur simultaneously and within seconds upon delivery of the flow pulse (Figures 3F and 3G). For both 86 and 1591, the cpGFP and jRGECO1a fluorescence signals are positively correlated during the duration of flow delivery, evidenced by Pearson's correlation coefficient values near unity (86: 0.86 ± 0.06, n = 8;

1591: 0.97 ± 0.01, n = 6) (Figure 3H). The two fluorescence signals appear uncorrelated before or after exposure to flow, showing that the positive correlation observed during flow is likely not caused artefactually, for instance by photon leakage across the spectrally separated optical paths collecting light from cpGFP and jRGECO1a.

PIEZO1 channels are expected to rapidly activate and inactivate upon sustained mechanical stimulation.[37,61] To investigate whether the cpGFP signals correlate with open or inactivated states, we introduced, in both 86 and 1591, pairs of mutations known to slow down or accelerate the rate of inactivation of macroscopic currents ($Tau_{inactivation}$). To slow down $Tau_{inactivation}$, we introduced M2241R and R2482H (MR-RH), which are murine homologs of human mutations M2225R (located in the cap) and R2456H (located in the inner pore helix), with each mutation slowing down inactivation.[63,64] The second pair consists of mPIEZO1 mutations L2475I and V2476I (LI-VI) (both located in the inner pore helix), which individually accelerate inactivation.[65] We first compared $Tau_{inactivation}$ between these new constructs and their unmodified parent constructs. Because the rate of PIEZO1 inactivation is slower at positive voltages,[3] we measured $Tau_{inactivation}$ at −80 and +80 mV. Introducing MR-RH in either 86 and 1591 slows down $Tau_{inactivation}$ by ∼1.5-fold at +80 mV and by ∼10-fold at −80 mV relative to their respective parent constructs, whereas inserting LI-VI in both 86 and 1591 accelerates $Tau_{inactivation}$ by ∼10-fold at +80 mV and by ∼2-fold at −80 mV relative to their respective parent constructs (Figures S2A–S2C). In addition, all constructs exhibit similar current density (Figure S2D).

If cpGFP dequenches only when the channels populate an open state, we expect the cpGFP signals to be attenuated by the fast-inactivating mutations. Reciprocally, if cpGFP dequenches only when the channels populate an inactivated state, we expect the cpGFP signals to be attenuated by the slow-inactivating mutations. Our data show that neither mutation pairs attenuate cpGFP signals either in 86 or in 1591 (Figures S2E and S2F). This suggests the hypothesis that the cpGFP signal develops concomitantly to pore opening and persists when inactivation sets in. For unclear reasons, the presence of the fast-inactivating LI-VI mutations correlates with brighter cpGFP signals in both 86 and 1591, seemingly due to the emergence of a slow fluorescence component, an effect that was more pronounced for 86 ($m\Delta F/F_0$ = 2.80 ± 0.35 vs. 0.33 ± 0.06 for control, $p < 0.0001$) than for 1591 ($m\Delta F/F_0$ = 1.12 ± 0.15 vs. 0.32 ± 0.11 for control, $p = 0.020$). This phenotype is likely not due to differences in channel expression, as current densities were similar among parental and mutated constructs (Figure S2F).

To investigate further the temporal correlation between cpGFP signals and PIEZO1's functional states, we multiplexed flow stimuli with whole-cell electrophysiology. Because our enclosed flow chambers are not compatible with patch-clamp recordings, we applied fluid shear stress through a nozzle, pumping HBSS through it using a syringe pump (see STAR Methods). Cells transfected with 86 or 1591, but not Lck-cpGFP, elicit cpGFP signals in response to a series of 4 consecutive flow pulses (10 s on/10 s off) of incrementally increasing amplitude (0.10, 0.36, 1, and 3.6 mL min^{-1}, corresponding to approximately 0.24, 0.87, 2.42, and 8.12 Pa; see STAR Methods) (Figure 4A). We next show that a single pulse of 0.36 mL min^{-1} (∼0.87 Pa) is sufficient to robustly dequench cpGFP in both 86 and 1591 but not Lck-cpGFP (Figures 4B–4D). In 86 and 1591, cpGFP signals clearly develop concomitantly to the rise of ionic currents but tend to persist when channels inactivate and even when the stimulus is subsequently removed, showing that our probes enable real-time tracking of conformational changes associated with channel activation but not those associated with subsequent inactivation.

We next sought to test the ability of both poke and flow to evoke cpGFP and ionic currents in the same cell. Cells were first activated by a 5 μm poke stimulus maintained for 10 s and, after a 20 s recovery period, by a 0.36 mL min^{-1} flow stimulus maintained for 10 s (Figure 4E). As observed earlier, the poke stimulus fails to elicit a cpGFP signal from either probe but does produce robust inward currents. On the other hand, the flow stimulus produces a robust cpGFP signal in cells transfected with either 86 or 1591 and simultaneously produces slowly activating/inactivating inward currents. Although these currents have a small peak amplitude compared with poke-induced currents, integration of these currents over the flow duration shows that they actually carry more charge than poke-induced currents (Figure 4F). The difference in total charge transported by the two stimuli may be due, at least in part, to the fact that the large nozzle inner diameter (0.838 mm) enables the flow stimulus to reach the entire cell surface, activating more channels than locally applied poke stimuli.

We noticed that high-intensity flow stimuli, which produce visible deformations of the cells, were not effective at eliciting cpGFP signals in 86 or 1591. To illustrate these observations, we plotted $m\Delta F/F_0$ obtained from cells stimulated through the nozzle with a single flow stimulus ranging from 0.01 (∼0.02 Pa) to 10 mL min^{-1} (∼24 Pa). Our data clearly show that, for both 86 and 1591, this plot has a distinctive bell-like shape, with the cpGFP signals having a maximum for flow rates between 0.1 and 1 mL min^{-1} (Figure 4G). Thus, only low-intensity flow stimuli are able to evoke cpGFP signals in 86 and 1591.

DISCUSSION

The PIEZO1 blades are known to undergo flattening motions in response to changes in membrane tension and/or curvature in artificial membrane systems or in computational simulations.[40,41,43,66] However, physiological mechanical stimuli may cause more complex mechanical deformations of the lipid bilayer, as they could apply a combination of tensional, compressional, and/or frictional stresses along different spatial directions relative to the cell membrane. Physiological mechanical stimuli may also regulate PIEZO1 activity by deforming the cytoskeleton, the extracellular matrix, and/or by modulating endogenous interactions with regulatory proteins.[67–75] It is thus still unclear how a physiological (osmotic stress, fluid shear stress) or a near-physiological (poking) mechanical stimulus physically deforms the cell membrane and/or its associated structural elements to activate PIEZOs.

A recent study shows that TRPA1 is selectively activated by shear stress but not by membrane tension nor poke stimuli.[76] This result mirrors the stimulus specificity captured by our cpGFP probes. Together, these observations show that at least

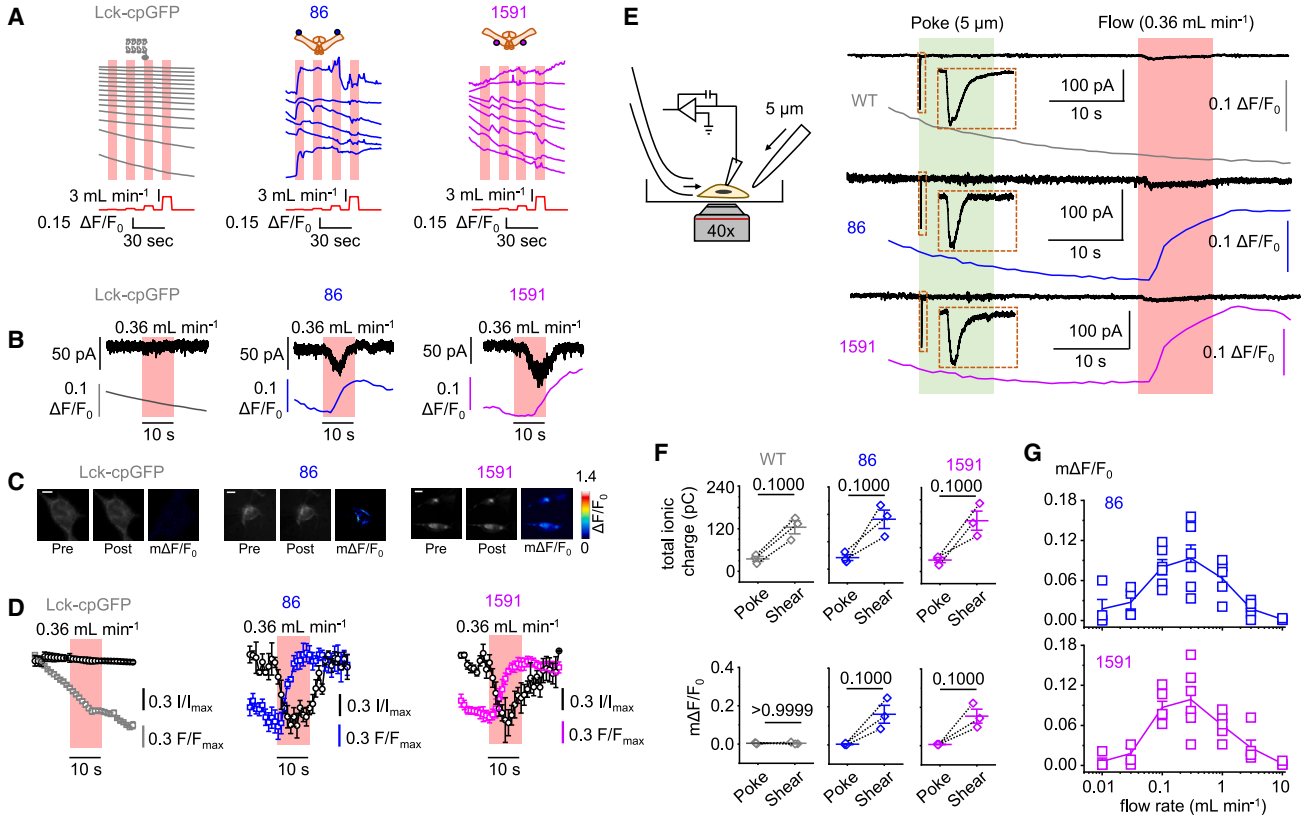

Figure 4. cpGFP signals in both 86 and 1591 correlate with PIEZO1 activation

(A) Representative cpGFP fluorescence traces from cells transfected with Lck-cpGFP, 86, or 1591 and exposed to a series of 4 escalating flow pulses (10 s/0.1–3.6 mL min^{-1}) delivered through an 18G nozzle.

(B) Representative simultaneous current (top) and fluorescence (bottom) recordings obtained in the same cell, transfected with either Lck-cpGFP, 86, or 1591 and acutely exposed to a 10 s/0.36 mL min^{-1} nozzle flow pulse.

(C) Representative images from cells stimulated as in (B). Scale bars represent 10 μm.

(D) Averaged normalized current and cpGFP fluorescence traces obtained from cells transfected with Lck-cpGFP (n = 8), 86 (n = 6), or 1591 (n = 4) and acutely exposed to a 10 s/0.36 mL min^{-1} nozzle flow pulse.

(E) Exemplar current and cpGFP fluorescence traces obtained from cells transfected with Lck-cpGFP, 86, or 1591 and stimulated by a 10 s/5 μm poke stimulus followed by a 10 s/0.36 mL min^{-1} nozzle flow pulse. A 20 s interval between two stimuli was used to enable channels to recover from inactivation.

(F) Scatterplots showing the time integral of ionic current (top) and $m\Delta F/F_0$ (bottom) from experiments depicted in (E).

(G) Scatterplots showing $m\Delta F/F_0$ values as a function of the flow rate used during a single 10 s nozzle flow pulse from cells transfected with 86 (top) or 1591 (bottom).

Each dot in (F) and (G) represents data from independent experiments. Numbers above plots in (F) indicate p values from Mann-Whitney U-tests. Error bars: SEM.

two unrelated membrane proteins can discriminate flow from other types of mechanical stimuli. Hence, mechanosensitive ion channels may have evolved specialized molecular pathways to detect different types of mechanical stress. This idea is further consistent with studies showing that certain mutations cause PIEZOs to lose sensitivity to a mechanical stimulus while maintaining normal sensitivity to others.[39,75]

How would low-intensity flow stimuli elicit distinct conformational changes in the PIEZO1 blades? The fact that the cpGFP signals strongly depend on the flow rate may give us a clue. While doing our experiments, we noticed that high-intensity flow stimuli produce visible membrane deformations, akin to those observed upon cellular indentations with a blunt glass pipette. Yet, neither of these stimuli cause our cpGFP probes to light up, suggesting that the low-intensity stimulus does not activate PIEZO by causing a large membrane deformation. It is possible that low-intensity flow stimuli act by producing a displacement of lipid molecules within the lipid bilayer or by disrupting lipid microdomains,[77,78] leading to a yet unclear conformational rearrangements of the blades. The distinctiveness of flow-induced conformational changes may not be strictly restricted to positions 86 and 1591, meaning that other regions of the blades could also discriminate mechanical stimuli. Future studies will be needed to elucidate in more structural detail how low-intensity flow stimuli rearrange this mechanosensory domain. This question is significant, since the amplitudes of shear stress at which our probes respond (and the channels open) is within the shear stress physiologically experienced by endothelial cells lining vascular and lymphatic capillaries as well as large veins.[79]

Do our cpGFP probes enable capturing a specific channel conformation? Our data show that the flow-induced cpGFP signals temporally correlate with the rise of ionic currents and calcium uptake. Yet, the cpGFP signals do not promptly decay when channels inactivate and are not attenuated by mutations that slow down or speed up the channel's inactivation rate, suggesting that the cpGFP probes detect movements of the blades associated with channel activation but do not detect subsequent conformational changes specifically associated with inactivation, which are predicted to occur in the pore and cap regions.[37,65] Yet, the presence of fast-inactivating mutations in the pore correlates with larger cpGFP signals. Hence, physical alterations in the pore region seem to influence the conformation of the blade upon mechanical stimulation. Reciprocally, a study has shown that optical gating of PIEZO1, achieved through isomerization of an azobenzene group genetically introduced into the pore,[80] is inhibited by the presence of disulfide bridges crosslinking the cap to the blades.[37] Together, these two observations suggest that protein motions in the PIEZO1 pore and blade domains are mutually (bidirectionally) coupled.

The persistence of fluorescence signals after flow removal is more puzzling. This persistence could be caused independently of the local conformational status of the protein backbone, for instance if the quenching kinetics (i.e., bright-to-dim transition) of the two cpGFP chromophores are slower than the kinetics of backbone conformational changes during inactivation/deactivation. However, cpGFP signals are rapidly reversible when inserted into a variety of host proteins activated by different stimuli.[49,50,55,81,82] On the other hand, the persistence of cpGFP signals could be due to the viscous nature of the interaction between fluid and membrane, which could maintain, at least partially, the mechanical stress long after removal of the flow stimulus. Evidence that this might be the case comes from our observation that channel kinetics are slower when evoked with our low-intensity flow stimulus compared with when they are evoked with patch pressurization or membrane indentation. This observation was also made by others, who have shown that the macroscopic currents from endogenous mechanosensitive ion channels in endothelial cells, including PIEZO1, have slow kinetics (~tens of seconds) when evoked by flow.[13,83,84]

Limitations of the study

Site-specific fluorimetry does not enable quantitative amplitude correlations between fluorimetric signals and backbone protein motions. In addition, fluorescence changes are predicted to occur across a small fraction of the possible conformational changes that may occur near the site of cpGFP insertion,[48] meaning that an absence of fluorimetric signal does not mean an absence of protein motion. Another limitation of this approach is the fact that the local conformation being probed could be affected by the presence of the cpGFP. Thus, one might argue that the conformational changes being probed are non-physiological. However, it would seem quite unlikely that inserting a cpGFP at two independent sites of the PIEZO1 blade, located ~20 nm apart according to the AlphaFold2 full-length PIEZO1 structural model,[85] bestows upon these two sites the ability to conformationally discriminate mechanical stimuli. If this was the case, our results would still show that two independently engineered channels discriminate low-intensity flow from other mechanical stimuli. This would still imply that low-intensity flow causes a unique form of mechanical stress to the cell, which, by itself, constitutes a noteworthy finding.

STAR★METHODS

Detailed methods are provided in the online version of this paper and include the following:

- KEY RESOURCES TABLE
- RESOURCE AVAILABILITY
  - Lead contact
  - Materials availability
  - Data and code availability
- EXPERIMENTAL MODEL AND STUDY PARTICIPANTS DETAILS
  - Cell line
- METHOD DETAILS
  - Molecular cloning
  - Cell culture and transfection
  - Fluorescence imaging
  - Image analysis
  - Cell indentation
  - Hypotonic shocks
  - Fluid shear stress stimulation and calculations
  - Electrophysiology
- QUANTIFICATION AND STATISTICAL ANALYSIS

SUPPLEMENTAL INFORMATION

Supplemental information can be found online at https://doi.org/10.1016/j.celrep.2023.112837.

ACKNOWLEDGMENTS

We thank Dr. Ibra Fancher (University of Delaware) for fruitful discussions. This work was supported by National Institutes of Health grant GM130834 to J.J.L.

AUTHOR CONTRIBUTIONS

J.J.L. conceived the project. A.D.O., T.D.W., T.G., and J.J.L. performed experiments. A.D.O., T.D.W., and J.J.L. analyzed data; J.J.L. wrote the manuscript with input from A.D.O. and T.D.W.

DECLARATION OF INTERESTS

The authors declare no competing interests.

INCLUSION AND DIVERSITY

We support inclusive, diverse, and equitable conduct of research.

Received: November 3, 2022
Revised: June 15, 2023
Accepted: July 5, 2023

REFERENCES

1. Syeda, R. (2021). Physiology and pathophysiology of mechanically activated PIEZO channels. Annu. Rev. Neurosci. *44*, 383–402. https://doi.org/10.1146/annurev-neuro-093020-120939.

2. Coste, B., Xiao, B., Santos, J.S., Syeda, R., Grandl, J., Spencer, K.S., Kim, S.E., Schmidt, M., Mathur, J., Dubin, A.E., et al. (2012). Piezo proteins are pore-forming subunits of mechanically activated channels. Nature *483*, 176–181. https://doi.org/10.1038/nature10812.

3. Coste, B., Mathur, J., Schmidt, M., Earley, T.J., Ranade, S., Petrus, M.J., Dubin, A.E., and Patapoutian, A. (2010). Piezo1 and Piezo2 are essential components of distinct mechanically activated cation channels. Science *330*, 55–60. https://doi.org/10.1126/science.1193270.

4. Cox, C.D., Bae, C., Ziegler, L., Hartley, S., Nikolova-Krstevski, V., Rohde, P.R., Ng, C.A., Sachs, F., Gottlieb, P.A., and Martinac, B. (2016). Removal of the mechanoprotective influence of the cytoskeleton reveals PIEZO1 is gated by bilayer tension. Nat. Commun. *7*, 10366. https://doi.org/10.1038/ncomms10366.

5. Lewis, A.H., and Grandl, J. (2015). Mechanical sensitivity of Piezo1 ion channels can be tuned by cellular membrane tension. Elife *4*, e12088. https://doi.org/10.7554/eLife.12088.

6. Syeda, R., Florendo, M.N., Cox, C.D., Kefauver, J.M., Santos, J.S., Martinac, B., and Patapoutian, A. (2016). Piezo1 channels are inherently mechanosensitive. Cell Rep. *17*, 1739–1746. https://doi.org/10.1016/j.celrep.2016.10.033.

7. Luo, M., K Y Ho, K., Tong, Z., Deng, L., and P Liu, A. (2019). Compressive stress enhances invasive phenotype of cancer cells via Piezo1 activation. Preprint at bioRxiv. https://doi.org/10.1101/513218.

8. Jetta, D., Gottlieb, P.A., Verma, D., Sachs, F., and Hua, S.Z. (2019). Shear stress-induced nuclear shrinkage through activation of Piezo1 channels in epithelial cells. J. Cell Sci. *132*, jcs226076. https://doi.org/10.1242/jcs.226076.

9. Wang, S., Chennupati, R., Kaur, H., Iring, A., Wettschureck, N., and Offermanns, S. (2016). Endothelial cation channel PIEZO1 controls blood pressure by mediating flow-induced ATP release. J. Clin. Invest. *126*, 4527–4536. https://doi.org/10.1172/JCI87343.

10. Ranade, S.S., Qiu, Z., Woo, S.H., Hur, S.S., Murthy, S.E., Cahalan, S.M., Xu, J., Mathur, J., Bandell, M., Coste, B., et al. (2014). Piezo1, a mechanically activated ion channel, is required for vascular development in mice. Proc. Natl. Acad. Sci. USA *111*, 10347–10352. https://doi.org/10.1073/pnas.1409233111.

11. Nonomura, K., Lukacs, V., Sweet, D.T., Goddard, L.M., Kanie, A., Whitwam, T., Ranade, S.S., Fujimori, T., Kahn, M.L., and Patapoutian, A. (2018). Mechanically activated ion channel PIEZO1 is required for lymphatic valve formation. Proc. Natl. Acad. Sci. USA *115*, 12817–12822. https://doi.org/10.1073/pnas.1817070115.

12. Choi, D., Park, E., Jung, E., Cha, B., Lee, S., Yu, J., Kim, P.M., Lee, S., Hong, Y.J., Koh, C.J., et al. (2019). Piezo1 incorporates mechanical force signals into the genetic program that governs lymphatic valve development and maintenance. JCI Insight *4*, e125068. https://doi.org/10.1172/jci.insight.125068.

13. Li, J., Hou, B., Tumova, S., Muraki, K., Bruns, A., Ludlow, M.J., Sedo, A., Hyman, A.J., McKeown, L., Young, R.S., et al. (2014). Piezo1 integration of vascular architecture with physiological force. Nature *515*, 279–282. https://doi.org/10.1038/nature13701.

14. Ellefsen, K.L., Chang, A., Nourse, J.L., Holt, J.R., Arulmoli, J., Mekhdjian, A., Aburwarda, H., Tombola, F., Flanagan, L.A., Dunn, A.R., et al. (2019). Myosin-II mediated traction forces evoke localized piezol Ca2+ flickers. Biophys. J. *116*, 377a. https://doi.org/10.1016/j.bpj.2018.11.2049.

15. Lacroix, J.J., Botello-Smith, W.M., and Luo, Y. (2018). Probing the gating mechanism of the mechanosensitive channel Piezo1 with the small molecule Yoda1. Nat. Commun. *9*, 2029. https://doi.org/10.1038/s41467-018-04405-3.

16. Gottlieb, P.A., Bae, C., and Sachs, F. (2012). Gating the mechanical channel Piezo1: a comparison between whole-cell and patch recording. Channels *6*, 282–289. https://doi.org/10.4161/chan.21064.

17. Poole, K., Herget, R., Lapatsina, L., Ngo, H.D., and Lewin, G.R. (2014). Tuning Piezo ion channels to detect molecular-scale movements relevant for fine touch. Nat. Commun. *5*, 3520. https://doi.org/10.1038/ncomms4520.

18. Koster, A.K., Wood, C.A.P., Thomas-Tran, R., Chavan, T.S., Almqvist, J., Choi, K.H., Du Bois, J., and Maduke, M. (2018). A selective class of inhibitors for the CLC-Ka chloride ion channel. Proc. Natl. Acad. Sci. USA *115*, E4900–E4909. https://doi.org/10.1073/pnas.1720584115.

19. Yoo, S., Mittelstein, D.R., Hurt, R.C., Lacroix, J., and Shapiro, M.G. (2022). Focused ultrasound excites cortical neurons via mechanosensitive calcium accumulation and ion channel amplification. Nat. Commun. *13*, 493. https://doi.org/10.1038/s41467-022-28040-1.

20. Zeng, W.Z., Marshall, K.L., Min, S., Daou, I., Chapleau, M.W., Abboud, F.M., Liberles, S.D., and Patapoutian, A. (2018). PIEZOs mediate neuronal sensing of blood pressure and the baroreceptor reflex. Science *362*, 464–467. https://doi.org/10.1126/science.aau6324.

21. Morley, L.C., Shi, J., Gaunt, H.J., Hyman, A.J., Webster, P.J., Williams, C., Forbes, K., Walker, J.J., Simpson, N.A.B., and Beech, D.J. (2018). Piezo1 channels are mechanosensors in human fetoplacental endothelial cells. Mol. Hum. Reprod. *24*, 510–520. https://doi.org/10.1093/molehr/gay033.

22. Hill, R.Z., Loud, M.C., Dubin, A.E., Peet, B., and Patapoutian, A. (2022). PIEZO1 transduces mechanical itch in mice. Nature *607*, 104–110. https://doi.org/10.1038/s41586-022-04860-5.

23. Gudipaty, S.A., Lindblom, J., Loftus, P.D., Redd, M.J., Edes, K., Davey, C.F., Krishnegowda, V., and Rosenblatt, J. (2017). Mechanical stretch triggers rapid epithelial cell division through Piezo1. Nature *543*, 118–121. https://doi.org/10.1038/nature21407.

24. Jiang, F., Yin, K., Wu, K., Zhang, M., Wang, S., Cheng, H., Zhou, Z., and Xiao, B. (2021). The mechanosensitive Piezo1 channel mediates heart mechano-chemo transduction. Nat. Commun. *12*, 869. https://doi.org/10.1038/s41467-021-21178-4.

25. Passini, F.S., Jaeger, P.K., Saab, A.S., Hanlon, S., Chittim, N.A., Arlt, M.J., Ferrari, K.D., Haenni, D., Caprara, S., Bollhalder, M., et al. (2021). Shear-stress sensing by PIEZO1 regulates tendon stiffness in rodents and influences jumping performance in humans. Nat. Biomed. Eng. *5*, 1457–1471. https://doi.org/10.1038/s41551-021-00716-x.

26. Nakamichi, R., Ma, S., Nonoyama, T., Chiba, T., Kurimoto, R., Ohzono, H., Olmer, M., Shukunami, C., Fuku, N., Wang, G., et al. (2022). The mechanosensitive ion channel PIEZO1 is expressed in tendons and regulates physical performance. Sci. Transl. Med. *14*, eabj5557. https://doi.org/10.1126/scitranslmed.abj5557.

27. Tadala, L., Langenbach, D., Dannborg, M., Cervantes-Rivera, R., Sharma, A., Vieth, K., Rieckmann, L.M., Wanders, A., Cisneros, D.A., and Puhar, A. (2022). Infection-induced membrane ruffling initiates danger and immune signaling via the mechanosensor PIEZO1. Cell Rep. *40*, 111173. https://doi.org/10.1016/j.celrep.2022.111173.

28. Wang, Y., Yang, H., Jia, A., Wang, Y., Yang, Q., Dong, Y., Hou, Y., Cao, Y., Dong, L., Bi, Y., and Liu, G. (2022). Dendritic cell Piezo1 directs the differentiation of TH1 and Treg cells in cancer. Elife *11*, e79957. https://doi.org/10.7554/eLife.79957.

29. Sun, W., Chi, S., Li, Y., Ling, S., Tan, Y., Xu, Y., Jiang, F., Li, J., Liu, C., Zhong, G., et al. (2019). The mechanosensitive Piezo1 channel is required for bone formation. Elife *8*, e47454. https://doi.org/10.7554/eLife.47454.

30. Li, X., Han, L., Nookaew, I., Mannen, E., Silva, M.J., Almeida, M., and Xiong, J. (2019). Stimulation of Piezo1 by mechanical signals promotes bone anabolism. Elife *8*, e49631. https://doi.org/10.7554/eLife.49631.

31. Saotome, K., Murthy, S.E., Kefauver, J.M., Whitwam, T., Patapoutian, A., and Ward, A.B. (2018). Structure of the mechanically activated ion channel Piezo1. Nature *554*, 481–486. https://doi.org/10.1038/nature25453.

32. Guo, Y.R., and MacKinnon, R. (2017). Structure-based membrane dome mechanism for Piezo mechanosensitivity. Elife *6*, e33660. https://doi.org/10.7554/eLife.33660.

33. Ge, J., Li, W., Zhao, Q., Li, N., Chen, M., Zhi, P., Li, R., Gao, N., Xiao, B., and Yang, M. (2015). Architecture of the mammalian mechanosensitive Piezo1 channel. Nature *527*, 64–69. https://doi.org/10.1038/nature15247.

34. Wang, L., Zhou, H., Zhang, M., Liu, W., Deng, T., Zhao, Q., Li, Y., Lei, J., Li, X., and Xiao, B. (2019). Structure and mechanogating of the mammalian tactile channel PIEZO2. Nature *573*, 225–229. https://doi.org/10.1038/s41586-019-1505-8.

35. Zhao, Q., Zhou, H., Chi, S., Wang, Y., Wang, J., Geng, J., Wu, K., Liu, W., Zhang, T., Dong, M.Q., et al. (2018). Structure and mechanogating mechanism of the Piezo1 channel. Nature *554*, 487–492. https://doi.org/10.1038/nature25743.

36. Nosyreva, E.D., Thompson, D., and Syeda, R. (2021). Identification and functional characterization of the Piezo1 channel pore domain. J. Biol. Chem. *296*, 100225. https://doi.org/10.1074/jbc.RA120.015905.

37. Lewis, A.H., and Grandl, J. (2020). Inactivation kinetics and mechanical gating of Piezo1 ion channels depend on subdomains within the cap. Cell Rep. *30*, 870–880.e2. https://doi.org/10.1016/j.celrep.2019.12.040.

38. Wu, J., Goyal, R., and Grandl, J. (2016). Localized force application reveals mechanically sensitive domains of Piezo1. Nat. Commun. *7*, 12939. https://doi.org/10.1038/ncomms12939.

39. Wang, Y., Chi, S., Guo, H., Li, G., Wang, L., Zhao, Q., Rao, Y., Zu, L., He, W., and Xiao, B. (2018). A lever-like transduction pathway for long-distance chemical- and mechano-gating of the mechanosensitive Piezo1 channel. Nat. Commun. *9*, 1300. https://doi.org/10.1038/s41467-018-03570-9.

40. Lin, Y.C., Guo, Y.R., Miyagi, A., Levring, J., MacKinnon, R., and Scheuring, S. (2019). Force-induced conformational changes in PIEZO1. Nature *573*, 230–234. https://doi.org/10.1038/s41586-019-1499-2.

41. Yang, X., Lin, C., Chen, X., Li, S., Li, X., and Xiao, B. (2022). Structure deformation and curvature sensing of PIEZO1 in lipid membranes. Nature *604*, 377–383. https://doi.org/10.1038/s41586-022-04574-8.

42. De Vecchis, D., Beech, D.J., and Kalli, A.C. (2021). Molecular dynamics simulations of Piezo1 channel opening by increases in membrane tension. Biophys. J. *120*, 1510–1521. https://doi.org/10.1016/j.bpj.2021.02.006.

43. Jiang, W., Del Rosario, J.S., Botello-Smith, W., Zhao, S., Lin, Y.C., Zhang, H., Lacroix, J., Rohacs, T., and Luo, Y.L. (2021). Crowding-induced opening of the mechanosensitive Piezo1 channel in silico. Commun. Biol. *4*, 84. https://doi.org/10.1038/s42003-020-01600-1.

44. Zhao, Q., Wu, K., Geng, J., Chi, S., Wang, Y., Zhi, P., Zhang, M., and Xiao, B. (2016). Ion permeation and mechanotransduction mechanisms of mechanosensitive piezo channels. Neuron *89*, 1248–1263. https://doi.org/10.1016/j.neuron.2016.01.046.

45. Dubin, A.E., Murthy, S., Lewis, A.H., Brosse, L., Cahalan, S.M., Grandl, J., Coste, B., and Patapoutian, A. (2017). Endogenous Piezo1 can confound mechanically activated channel identification and characterization. Neuron *94*, 266–270.e3. https://doi.org/10.1016/j.neuron.2017.03.039.

46. Cowgill, J., and Chanda, B. (2019). The contribution of voltage clamp fluorometry to the understanding of channel and transporter mechanisms. J. Gen. Physiol. *151*, 1163–1172. https://doi.org/10.1085/jgp.201912372.

47. Wulf, M., and Pless, S.A. (2018). High-sensitivity fluorometry to resolve ion channel conformational dynamics. Cell Rep. *22*, 1615–1626. https://doi.org/10.1016/j.celrep.2018.01.029.

48. Nasu, Y., Shen, Y., Kramer, L., and Campbell, R.E. (2021). Structure- and mechanism-guided design of single fluorescent protein-based biosensors. Nat. Chem. Biol. *17*, 509–518. https://doi.org/10.1038/s41589-020-00718-x.

49. Ozkan, A.D., Gettas, T., Sogata, A., Phaychanpheng, W., Zhou, M., and Lacroix, J.J. (2021). Mechanical and chemical activation of GPR68 probed with a genetically encoded fluorescent reporter. J. Cell Sci. *134*, jcs255455. https://doi.org/10.1242/jcs.255455.

50. Patriarchi, T., Cho, J.R., Merten, K., Howe, M.W., Marley, A., Xiong, W.H., Folk, R.W., Broussard, G.J., Liang, R., Jang, M.J., et al. (2018). Ultrafast neuronal imaging of dopamine dynamics with designed genetically encoded sensors. Science *360*, eaat4422. https://doi.org/10.1126/science.aat4422.

51. Dong, C., Ly, C., Dunlap, L.E., Vargas, M.V., Sun, J., Hwang, I.W., Azinfar, A., Oh, W.C., Wetsel, W.C., Olson, D.E., and Tian, L. (2021). Psychedelic-inspired drug discovery using an engineered biosensor. Cell *184*, 2779–2792.e18. https://doi.org/10.1016/j.cell.2021.03.043.

52. Chamberland, S., Yang, H.H., Pan, M.M., Evans, S.W., Guan, S., Chavarha, M., Yang, Y., Salesse, C., Wu, H., Wu, J.C., et al. (2017). Fast two-photon imaging of subcellular voltage dynamics in neuronal tissue with genetically encoded indicators. Elife *6*, e25690. https://doi.org/10.7554/eLife.25690.

53. Dong, A., He, K., Dudok, B., Farrell, J.S., Guan, W., Liput, D.J., Puhl, H.L., Cai, R., Wang, H., Duan, J., et al. (2022). A fluorescent sensor for spatiotemporally resolved imaging of endocannabinoid dynamics in vivo. Nat. Biotechnol. *40*, 787–798. https://doi.org/10.1038/s41587-021-01074-4.

54. Miyawaki, A., Llopis, J., Heim, R., McCaffery, J.M., Adams, J.A., Ikura, M., and Tsien, R.Y. (1997). Fluorescent indicators for Ca2+ based on green fluorescent proteins and calmodulin. Nature *388*, 882–887. https://doi.org/10.1038/42264.

55. St-Pierre, F., Marshall, J.D., Yang, Y., Gong, Y., Schnitzer, M.J., and Lin, M.Z. (2014). High-fidelity optical reporting of neuronal electrical activity with an ultrafast fluorescent voltage sensor. Nat. Neurosci. *17*, 884–889. https://doi.org/10.1038/nn.3709.

56. Syeda, R., Xu, J., Dubin, A.E., Coste, B., Mathur, J., Huynh, T., Matzen, J., Lao, J., Tully, D.C., Engels, I.H., et al. (2015). Chemical activation of the mechanotransduction channel Piezo1. Elife *4*, e07369. https://doi.org/10.7554/eLife.07369.

57. Lukacs, V., Mathur, J., Mao, R., Bayrak-Toydemir, P., Procter, M., Cahalan, S.M., Kim, H.J., Bandell, M., Longo, N., Day, R.W., et al. (2015). Impaired PIEZO1 function in patients with a novel autosomal recessive congenital lymphatic dysplasia. Nat. Commun. *6*, 8329. https://doi.org/10.1038/ncomms9329.

58. Dana, H., Mohar, B., Sun, Y., Narayan, S., Gordus, A., Hasseman, J.P., Tsegaye, G., Holt, G.T., Hu, A., Walpita, D., et al. (2016). Sensitive red protein calcium indicators for imaging neural activity. Elife *5*, e12727. https://doi.org/10.7554/eLife.12727.

59. Parsonage, G., Cuthbertson, K., Endesh, N., Murciano, N., Hyman, A.J., Revill, C.H., Povstyan, O.V., Chuntharpursat-Bon, E., Debant, M., Ludlow, M.J., et al. (2023). Improved PIEZO1 agonism through 4-benzoic acid modification of Yoda1. Br. J. Pharmacol. https://doi.org/10.1111/bph.15996.

60. Evans, E.L., Cuthbertson, K., Endesh, N., Rode, B., Blythe, N.M., Hyman, A.J., Hall, S.J., Gaunt, H.J., Ludlow, M.J., Foster, R., and Beech, D.J. (2018). Yoda1 analogue (Dooku1) which antagonizes Yoda1-evoked activation of Piezo1 and aortic relaxation. Br. J. Pharmacol. *175*, 1744–1759. https://doi.org/10.1111/bph.14188.

61. Wijerathne, T.D., Ozkan, A.D., and Lacroix, J.J. (2022). Yoda1's energetic footprint on Piezo1 channels and its modulation by voltage and temperature. Proc. Natl. Acad. Sci. USA *119*, e2202269119. https://doi.org/10.1073/pnas.2202269119.

62. Fregin, B., Biedenweg, D., and Otto, O. (2022). Interpretation of cell mechanical experiments in microfluidic systems depend on the choice of cellular shape descriptors. Biomicrofluidics *16*, 024109. https://doi.org/10.1063/5.0084673.

63. Andolfo, I., Alper, S.L., De Franceschi, L., Auriemma, C., Russo, R., De Falco, L., Vallefuoco, F., Esposito, M.R., Vandorpe, D.H., Shmukler, B.E., et al. (2013). Multiple clinical forms of dehydrated hereditary stomatocytosis arise from mutations in PIEZO1. Blood *121*, 3925–3935, S1-S12, S3921-S3912. https://doi.org/10.1182/blood-2013-02-482489.

64. Bae, C., Gnanasambandam, R., Nicolai, C., Sachs, F., and Gottlieb, P.A. (2013). Xerocytosis is caused by mutations that alter the kinetics of the mechanosensitive channel PIEZO1. Proc. Natl. Acad. Sci. USA *110*, E1162–E1168. https://doi.org/10.1073/pnas.1219777110.

65. Zheng, W., Gracheva, E.O., and Bagriantsev, S.N. (2019). A hydrophobic gate in the inner pore helix is the major determinant of inactivation in

mechanosensitive Piezo channels. Elife *8*, e44003. https://doi.org/10.7554/eLife.44003.

66. Haselwandter, C.A., and MacKinnon, R. (2018). Piezo's membrane footprint and its contribution to mechanosensitivity. Elife *7*, e41968. https://doi.org/10.7554/eLife.41968.
67. Wang, J., Jiang, J., Yang, X., Zhou, G., Wang, L., and Xiao, B. (2022). Tethering Piezo channels to the actin cytoskeleton for mechanogating via the cadherin-beta-catenin mechanotransduction complex. Cell Rep. *38*, 110342. https://doi.org/10.1016/j.celrep.2022.110342.
68. Mylvaganam, S., Plumb, J., Yusuf, B., Li, R., Lu, C.Y., Robinson, L.A., Freeman, S.A., and Grinstein, S. (2022). The spectrin cytoskeleton integrates endothelial mechanoresponses. Nat. Cell Biol. *24*, 1226–1238. https://doi.org/10.1038/s41556-022-00953-5.
69. Nourse, J.L., and Pathak, M.M. (2017). How cells channel their stress: interplay between Piezo1 and the cytoskeleton. Semin. Cell Dev. Biol. *71*, 3–12. https://doi.org/10.1016/j.semcdb.2017.06.018.
70. Ellefsen, K.L., Holt, J.R., Chang, A.C., Nourse, J.L., Arulmoli, J., Mekhdjian, A.H., Abuwarda, H., Tombola, F., Flanagan, L.A., Dunn, A.R., et al. (2019). Myosin-II mediated traction forces evoke localized Piezo1-dependent Ca(2+) flickers. Commun. Biol. *2*, 298. https://doi.org/10.1038/s42003-019-0514-3.
71. Lai, A., Thurgood, P., Cox, C.D., Chheang, C., Peter, K., Jaworowski, A., Khoshmanesh, K., and Baratchi, S. (2022). Piezo1 response to shear stress is controlled by the components of the extracellular matrix. ACS Appl. Mater. Interfaces *14*, 40559–40568. https://doi.org/10.1021/acsami.2c09169.
72. Gaub, B.M., and Müller, D.J. (2017). Mechanical stimulation of Piezo1 receptors depends on extracellular matrix proteins and directionality of force. Nano Lett. *17*, 2064–2072. https://doi.org/10.1021/acs.nanolett.7b00177.
73. Wang, J., Jiang, J., Yang, X., Wang, L., and Xiao, B. (2020). Tethering Piezo channels to the actin cytoskeleton for mechanogating via the E-cadherin-β-catenin mechanotransduction complex. Preprint at bioRxiv. https://doi.org/10.1101/2020.05.12.092148.
74. Zhang, T., Chi, S., Jiang, F., Zhao, Q., and Xiao, B. (2017). A protein interaction mechanism for suppressing the mechanosensitive Piezo channels. Nat. Commun. *8*, 1797. https://doi.org/10.1038/s41467-017-01712-z.
75. Verkest, C., Schaefer, I., Nees, T.A., Wang, N., Jegelka, J.M., Taberner, F.J., and Lechner, S.G. (2022). Intrinsically disordered intracellular domains control key features of the mechanically-gated ion channel PIEZO2. Nat. Commun. *13*, 1365. https://doi.org/10.1038/s41467-022-28974-6.
76. Gong, J., Nirala, N.K., Chen, J., Wang, F., Gu, P., Wen, Q., Ip, Y.T., and Xiang, Y. (2023). TrpA1 is a shear stress mechanosensing channel regulating intestinal stem cell proliferation in Drosophila. Sci. Adv. *9*, eadc9660. https://doi.org/10.1126/sciadv.adc9660.
77. Buyan, A., Cox, C.D., Barnoud, J., Li, J., Chan, H.S.M., Martinac, B., Marrink, S.J., and Corry, B. (2020). Piezo1 forms specific, functionally important interactions with phosphoinositides and cholesterol. Biophys. J. *119*, 1683–1697. https://doi.org/10.1016/j.bpj.2020.07.043.
78. Ridone, P., Pandzic, E., Vassalli, M., Cox, C.D., Macmillan, A., Gottlieb, P.A., and Martinac, B. (2020). Disruption of membrane cholesterol organization impairs the activity of PIEZO1 channel clusters. J. Gen. Physiol. *152*, e201912515. https://doi.org/10.1085/jgp.201912515.
79. Ballermann, B.J., Dardik, A., Eng, E., and Liu, A. (1998). Shear stress and the endothelium. Kidney Int. Suppl. *67*, S100–S108. https://doi.org/10.1046/j.1523-1755.1998.06720.x.
80. Peralta, F.A., Balcon, M., Martz, A., Biljali, D., Cevoli, F., Arnould, B., Taly, A., Chataigneau, T., and Grutter, T. (2023). Optical control of PIEZO1 channels. Nat. Commun. *14*, 1269. https://doi.org/10.1038/s41467-023-36931-0.
81. Nagai, T., Sawano, A., Park, E.S., and Miyawaki, A. (2001). Circularly permuted green fluorescent proteins engineered to sense Ca2+. Proc. Natl. Acad. Sci. USA *98*, 3197–3202. https://doi.org/10.1073/pnas.051636098.
82. Feng, J., Zhang, C., Lischinsky, J.E., Jing, M., Zhou, J., Wang, H., Zhang, Y., Dong, A., Wu, Z., Wu, H., et al. (2019). A genetically encoded fluorescent sensor for rapid and specific in vivo detection of norepinephrine. Neuron *102*, 745–761.e8. https://doi.org/10.1016/j.neuron.2019.02.037.
83. Shi, J., Hyman, A.J., De Vecchis, D., Chong, J., Lichtenstein, L., Futers, T.S., Rouahi, M., Salvayre, A.N., Auge, N., Kalli, A.C., and Beech, D.J. (2020). Sphingomyelinase disables inactivation in endogenous PIEZO1 channels. Cell Rep. *33*, 108225. https://doi.org/10.1016/j.celrep.2020.108225.
84. Olesen, S.P., Clapham, D.E., and Davies, P.F. (1988). Haemodynamic shear stress activates a K+ current in vascular endothelial cells. Nature *331*, 168–170. https://doi.org/10.1038/331168a0.
85. Jumper, J., Evans, R., Pritzel, A., Green, T., Figurnov, M., Ronneberger, O., Tunyasuvunakool, K., Bates, R., Žídek, A., Potapenko, A., et al. (2021). Highly accurate protein structure prediction with AlphaFold. Nature *596*, 583–589. https://doi.org/10.1038/s41586-021-03819-2.
86. Cha, M., Ling, J., Xu, G.Y., and Gu, J.G. (2011). Shear mechanical force induces an increase of intracellular Ca2+ in cultured Merkel cells prepared from rat vibrissal hair follicles. J. Neurophysiol. *106*, 460–469. https://doi.org/10.1152/jn.00274.2011.

STAR★METHODS

KEY RESOURCES TABLE

REAGENT or RESOURCE	SOURCE	IDENTIFIER
Chemicals, peptides, and recombinant proteins		
Polyvinylpyrrolidone (MW = 360,000)	Sigma-Aldrich	PVP360-100G Lot #WXBC8456V
Deposited data		
Fluorescence traces	Open Science Framework	https://osf.io/94f8m/
		https://doi.org/10.17605/OSF.IO/94F8M
Experimental models: Cell lines		
HEK293T$^{\Delta PZ1}$ (Piezo1 knock-out HEK293T) recombinant human embryonic kidney cells	Lukacs et al.[57]	ATCC #CRL-3519
Oligonucleotides		
See Table S1 for a list of primer sequences		N/A
Recombinant DNA		
pCDNA3.1-ASAP1	St-Pierre et al.[55]	RRID: Addgene_52519
pCDNA3.1-jRGECO1a	Ozkan et al.[49] Dana et al.[58]	Cloned from RRID: Addgene_61563
Software and algorithms		
MATLAB code to quantify fluorescence intensity	GitHub	https://github.com/LacroixLaboratory/Force-induced-motions-of-the-PIEZO1-blade-probed-with-fluorimetry-
		https://doi.org/10.5281/zenodo.8117561

RESOURCE AVAILABILITY

Lead contact

Further information and requests for resources and reagents should be directed to and will be fulfilled by the Lead Contact, Jérôme J. Lacroix (jlacroix@westernu.edu).

Materials availability

All plasmids generated in this study are available from the lead contact with a completed materials transfer agreement.

Data and code availability

- Fluorescence data have been deposited at Open Science Framework and are publicly available as of the date of publication. Accession numbers are listed in the key resources table.
- All original code has been deposited at https://github.com/LacroixLaboratory and is publicly available as of the date of publication. DOIs are listed in the key resources table.
- Any additional information required to reanalyze the data reported in this paper is available from the lead contact upon request.

EXPERIMENTAL MODEL AND STUDY PARTICIPANTS DETAILS

Cell line

HEK293T$^{\Delta PZ1}$ cells are derived from human female embryonic kidney cells and lack endogenous PIEZO1 expression. The sex of these cells is not anticipated to influence our results. These cells were gifted to us by Dr. Patapoutian (Scripps Research) and were not further authenticated. These cells were cultured in standard conditions (37°C, 5% CO_2) in a Dulbecco's Modified Eagle's Medium supplemented with Penicillin (100 U mL^{-1}), streptomycin (0.1 mg mL^{-1}), 10% sterile Fetal Bovine Serum without L-glutamine. These reagents were purchased from Sigma-Aldrich.

METHOD DETAILS

Molecular cloning

A pCDNA3.1-mPIEZO1 plasmid was generously donated by Dr. Ardèm Patapoutian (Scripps Research). cpGFP fragments were PCR-amplified from a pCDNA3.1-ASAP1 plasmid gifted by Dr. Francois Saint-Pierre (Baylor College of Medicine & Rice University) and inserted to desired positions into the pCDNA.3.1-mPIEZO1 plasmid using High-Fidelity DNA Assembly (New England Biolabs). The presence of cpGFP inserts was confirmed by Sanger sequencing (GENEWIZ). The pCDNA3.1-jRGECO1a plasmid was obtained from a previous study.[49] The double mutants M2241R-R2482H and L2475I-V2476I were inserted into pCDNA3.1-mPIEZO1-cpGF86 and pCDNA3.1-mPIEZO1-cpGF1591 using High-Fidelity DNA Assembly and verified by Sanger sequencing.

Cell culture and transfection

Plasmids were transfected in cells (passage number <35) seeded in 96-well plates at ~50% confluence 2–4 days before the experiment with FuGene6 (Promega) or Lipofectamine 2000/3000 following the manufacturer's instructions. 1–2 days before experiments, cells were gently detached by 5 min incubation with Phosphate Buffer Saline and re-seeded onto 18 mm round glass coverslips (Warner Instruments) coated with Matrigel (Corning) or onto single or six-channels microfluidic devices (Ibidi μ-slides VI 0.4 or μ-slides I 0.4).

Fluorescence imaging

Cell culture medium was replaced with HBSS approximately 20 min before imaging experiments. Excitation light was generated by a Light Emitting Diode light engine (Spectra X, Lumencor), cleaned through individual single-band excitation filters (Semrock) and sent to the illumination port of an inverted fluorescence microscope (IX73, Olympus) by a liquid guide light. Excitation light was reflected onto the back focal plane of a plan super apochromatic 100X oil-immersion objective with 1.4 numerical aperture (Olympus) using a triple-band dichroic mirror (FF403/497/574, Semrock). Fluorescence emission from emerald-color transfected cells was filtered through a triple-band emission filter (FF01-433/517/613, Semrock) and sent through beam-splitting optics (W-View Gemini, Hamamatsu). Split and unsplit fluorescence images were collected by a sCMOS (Zyla 4.2) or by an emCCD (iXon Ultra 897) ANDOR camera (Oxford Instruments). Spectral separation by the Gemini was done using flat imaging dichroic mirrors and emission filters (Semrock). Images were collected by the Solis software (Oxford Instruments) at a rate of 1 frame s^{-1} or 10 frames s^{-1} (for poking experiments). Image acquisition and sample illumination were synchronized using TTL triggers digitally generated by the Clampex software (Molecular Devices). To reduce photobleaching, samples were pulse-illuminated 200 ms per frame during acquisition.

Image analysis

The first frame of each image stack was initially pre-processed in ImageJ by manually drawing individual cell boundaries and cropping out all background pixels. This mask was then used to define each cell as a unique region of interest. An in-house MATLAB script was then used to determine the average intensity of all pixels associated with each cell, F, and determine $m\Delta F/F_0$ value for each cell across the trajectory.

Cell indentation

Premium standard wall borosilicate capillaries 1.5mm x 4 in (Warner Instruments) were heat-pulled on a horizontal puller (Sutter P-97) and fire-polished on a microforge (Narishige MF-900) to produce smooth and round poking probes with tip diameter 2–5 μm. Poking probes were directly mounted onto a closed-loop piezoelectric actuator (LVPZT, Physik Instrumente) attached to a micromanipulator (MP-225, Sutter Instruments). Probes were moved as close to the surface of the cell as possible at an angle of approximately 60° and without physical contact. This initial position corresponds to a 0 μm displacement. Probes were linearly displaced in their longitudinal axis at a speed of ~0.1 μm ms^{-1} using an LVPZT amplifier (E−625.SR, Physik Instrumente) and external voltage triggers commanded by Clampex.

Hypotonic shocks

During image acquisition, the extracellular recording solution (HBSS) from cultured dishes was replaced with a hypotonic solution containing 5 mM NaCl, 5 mM KCl, 2 mM $MgCl_2$, 1 mM $CaCl_2$, 10 mM HEPES (pH 7.4 with HCl or NaOH) and 10 mM Glucose. The osmolarity of the hypotonic solution (~58 mOsmol L^{-1}) was measured by a micro-sample osmometer (Advanced Instruments Fiske 210).

Fluid shear stress stimulation and calculations

Two delivery methods were used. For non-electrophysiology experiments, we used 0.4 mm height μ-slide flow chambers (Ibidi) connected to a peristaltic pump (Golander) or a syringe pump (NE-1000, New Era Pump Systems). Each pump was TTL-controlled by Clampex. The average amplitude of wall shear stress τ applied at the cell surface was estimated using Ibidi's empirical equation relating shear stress, τ (Pa), with flow rate Φ (mL min^{-1}) and dynamic viscosity η (Pa s): $\tau = \eta \times 13.16 \times \Phi$. A η value of 0.001 Pa s was used for HBSS at room temperature. For electrophysiology experiments, an HBSS solution supplemented with 2% polyvinylpyrrolidone (Sigma-Aldrich, Molecular weight = 360,000) was delivered at variable flow rates powered by AL-1000 Syringe Pump

(WPI, USA) to individual cells through a 18-gauge canula positioned at the bottom of, and parallel to, the coverslip, and located less than ~0.1 mm from the cell. The shear stress produced by this stimulus was estimated from Poiseuille's law by: $\tau = \frac{4\eta\Phi}{\pi R^3}$[84,86], with τ the shear stress in dyn cm^{-2} (1 dyn cm^{-2} = 0.1 Pa), Φ the flow rate in mL s^{-1}, R the inner nozzle radius (0.419 mm), and η (0.08 Pa s) the viscosity measured at room temperature in our lab using a rotary viscometer (U.S. SOLID).

Electrophysiology

Cells were used 2–3 days after transfection. Pipettes were pulled from thin-wall borosilicate capillaries with internal filament (GC 150TF-7.5, Harvard Apparatus) to a resistance of 2–3 MΩ using a vertical pipette puller PC-10 (Narishige). Pipettes were filled with an internal solution containing 140 mM KCl, 10 HEPES, 10 mM TEA and 2 mM EGTA (pH 7.4 with NaOH), whereas HBSS (GIBCO) was used as bath solution. Transfected cells were placed onto an inverted microscope (Olympus IX73) mounted on an air table (TMC). Experiments were performed at room temperature using an Axopatch 200B capacitor-feedback patch clamp amplifier (Molecular Devices) connected to a Digidata 1550B low-noise data acquisition system plus hum silencer (Molecular Devices) and controlled using the Clampex software (Molecular Devices). For cell-attached pressure-clamp recordings, negative pressure stimuli were delivered to the backside of patch pipettes using a Clampex-controlled high-speed pressure clamp (ALA Scientific Instruments, USA). Resting membrane potential of the transfected cells was -28 ± 5 mV when measured using the above-mentioned saline solutions. Therefore, a +50/−110 mV holding potential was applied through the pipette electrode to provide $\sim -80/+80$ mV potential across the membrane patch. For whole-cell poking recordings, pipettes were fire polished using a microforge (MF2, Narishige) and indentation stimuli were delivered as described above. Currents were acquired using a sampling rate of 500 kHz and a filtering frequency of 5 kHz. Data were subsequently filtered at 500 Hz for display. Voltage clamp fluorometry (concurrent florescence patch clamp recording) was done by combining the patch clamp setup with the fluorescence imaging setup described under ''Fluorescence imaging''. Image acquisition and patch clamp protocols are identical to the protocols described in previous paragraphs. The camera, light engine and syringe pump were connected to the same Digidata 1550B low-noise data acquisition (Molecular Devices) and controlled using the Clampex software (Molecular Devices) used for patch clamp experiments.

QUANTIFICATION AND STATISTICAL ANALYSIS

We used non-parametric Kruskal-Wallis (with Dunn's multiple comparison p value corrections) and Mann-Whitney U-tests to compare experimental groups as sample size was generally not large enough to unambiguously follow a normal distribution. All statistical analyses were performed on GraphPad Prism 9.0. For fluorimetry experiments, sample size values (n) indicate single cells or clusters of transfected cells which typically produce identical responses. For electrophysiology, n represents the number of patched cells. Mid-point activation for poke and stretch recordings were obtained using a standard Boltzmann fitting (Origin Pro). All error bars are standard errors of the mean. Exact p values are reported for each test and a typical threshold of 5% is used for statistical significance and data interpretation.

Cell Reports, Volume *42*

Supplemental information

Force-induced motions of the PIEZO1 blade probed with fluorimetry

Alper D. Ozkan, Tharaka D. Wijerathne, Tina Gettas, and Jérôme J. Lacroix

Gibson Assembly constructs	Template	5'→3' forward primer	5'→3' reverse primer
mPIEZO1-cpGFP-86	ASAP1	gcctacacaccgtgcctcaaacgtgtatattaccgcg	ccagaaactggtccaggttatattccagtttatgccc
	pCDNA3.1-mPIEZO1	ctggaccagtttctgggacaaaacgg	tgaggcacggtgtgtaggc
mPIEZO1-cpGFP-300	ASAP1	cgaagttcttgagaccaacgtgtatattaccgcg	gctggagtagttagggttatattccagtttatgccc
	pCDNA3.1-mPIEZO1	cctaactactccagcccc	ggtctcaagaacttcgtagacctc
mPIEZO1-cpGFP-656	ASAP1	gtgtacaccttccagttccagaacgtgtatattaccgcg	taggtggggaagtcgttatattccagtttatgccc
	pCDNA3.1-mPIEZO1	gacttccccacctattgg	ctggaactggaaggtgtacac
mPIEZO1-cpGFP-1299	ASAP1	cggcgcatctttctcagcaacgtgtatattaccgcg	atgcaggaagtagtggttatattccagtttatgccc
	pCDNA3.1-mPIEZO1	cactacttcctgcatgtcagcg	gcaacggcgcatctttctcagc
mPIEZO1-cpGFP-1591	ASAP1	tgggagccgaagagcctttgaacgtgtatattaccgcg	gtgtcgtctgtcatgctactgttatattccagtttatgccc
	pCDNA3.1-mPIEZO1	agtagcatgacagacgacaccagcagc	caaaggctcttcggctcc
Point mutagenesis constructs	**Template**	**5'→3' forward primer**	**5'→3' reverse primer**
L2475I V2476I	mPIEZO1-cpGFP-86/1591	tctccatcgtgatcatcgttggcaagtttg	caaacttgccaacgatgatcacgatggaga
M2241R	mPIEZO1-cpGFP-86/1591	ccactgttcaccaggagcgcccagcagc	gctgctgggcgctcctggtgaacagtgg
R2482H	mPIEZO1-cpGFP-86/1591	ggcaagtttgtgcacggcttcttcagcg	cgctgaagaagccgtgcacaaacttgcc

Table S1. Oligonucleotidic sequences of primers used in this study, related to Figures 1-4. Gibson Assembly primers were used to transplant cpGFP from ASAP1 to the indicated PIEZO1 positions. Point mutagenesis primers were used to introduce points mutations in constructs 86 and 1591.

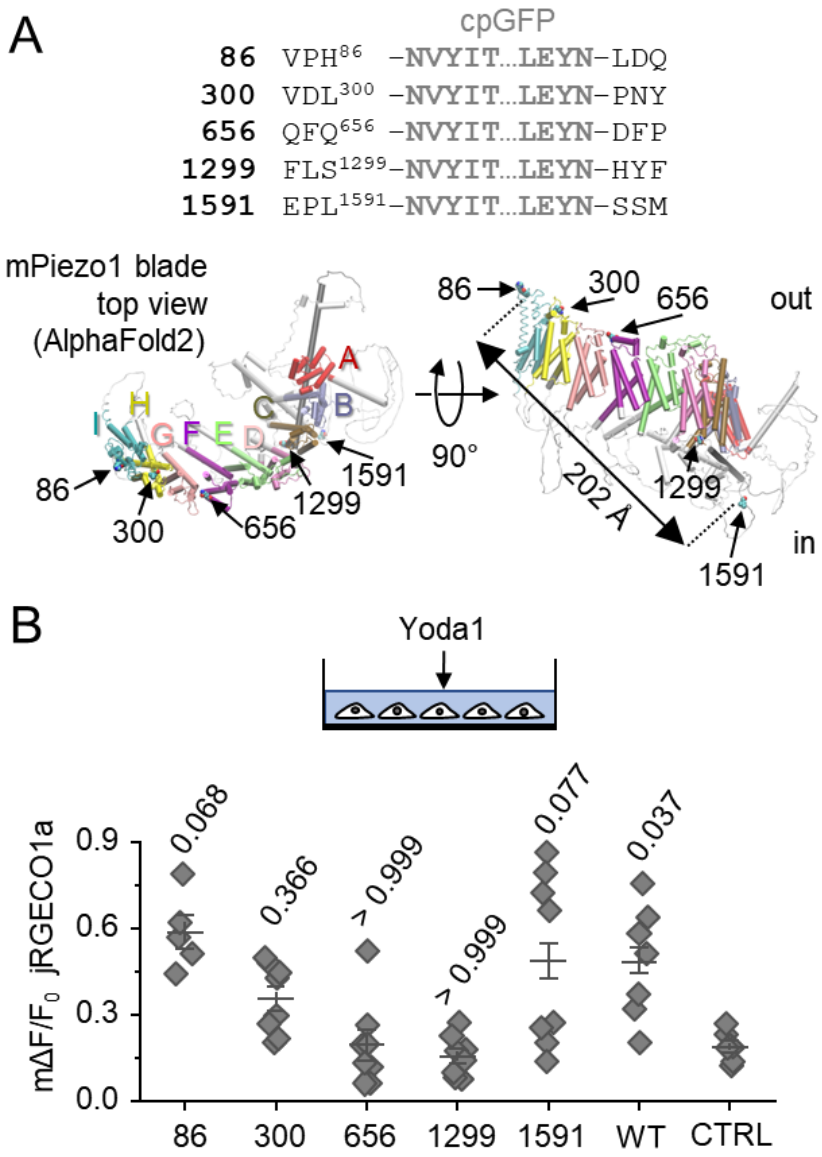

Figure S1. Selection of functional cpGFP constructs, related to Figure 1. (**A**) *Top*: amino acid sequences showing cpGFP insertion sites into mPIEZO1. *Bottom*: position of cpGFP insertion sites in the full-length AlphaFold2 structural model of the mPIEZO1 blade (letters and coloring indicate PIEZO repeats A to I). The structure also indicates the Cα-Cα distance between H86 and L1591. (**B**) Maximal calcium response ($m\Delta F/F_0$) to acute perfusion with 100 µM Yoda1 from HEK293T$^{\Delta PZ1}$ cells transfected with the jRGECO1a plasmid only (CTRL: n = 7) or co-transfected with plasmids encoding the indicated constructs (86: n = 5; 300: n = 8; 656: n = 8; 1299: n = 8: 1591: n = 7; WT mPIEZO1: n = 7). Each dot corresponds to the mean $m\Delta F/F_0$ value obtained from at least 20 cells from n wells. Numbers above bars indicate p-values from Kruskal-Wallis tests with Dunn's multiple comparisons against control. Error bars = s.e.m.

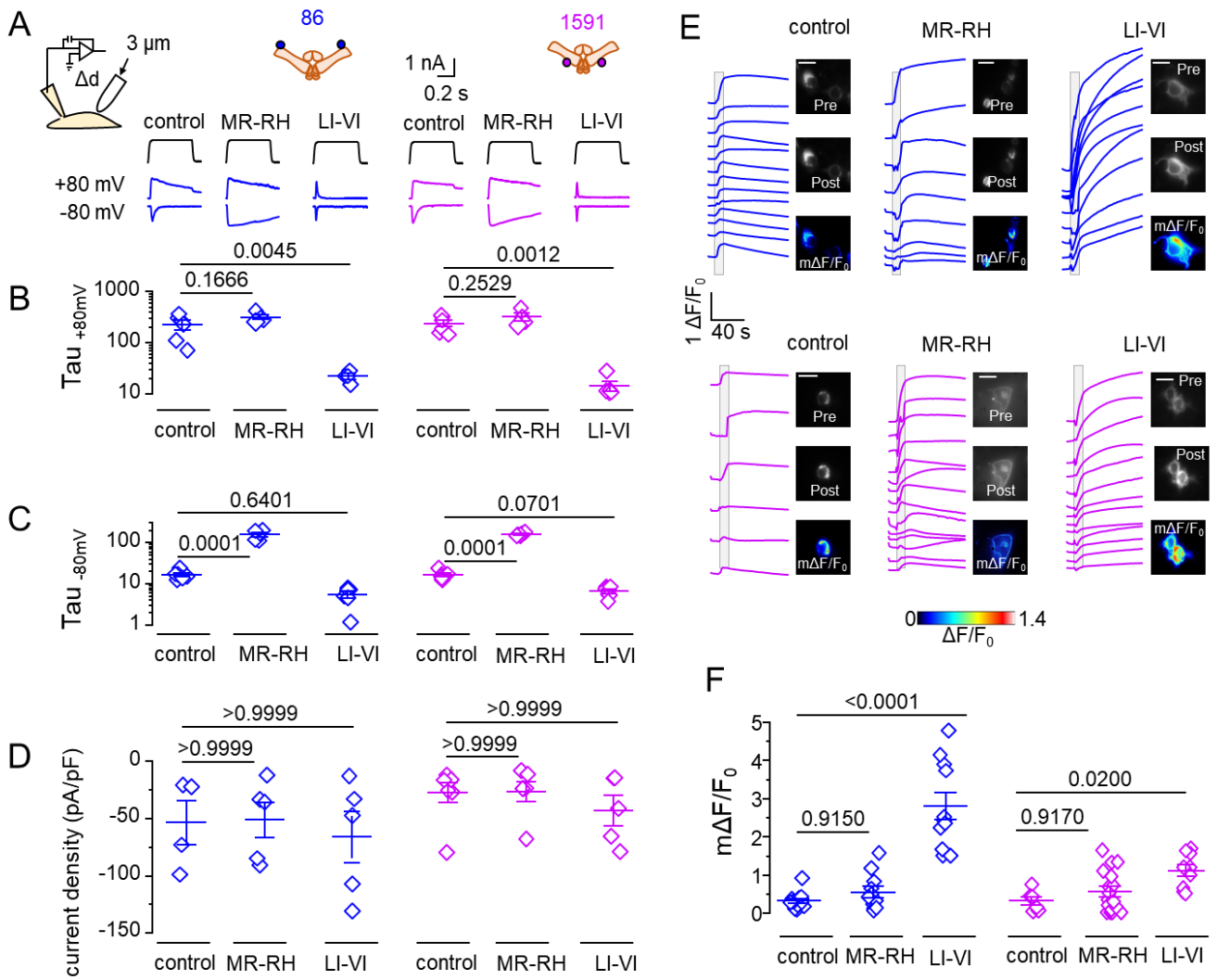

Figure S2. Modulation of cpGFP signals by mutations modulating inactivation, related to Figures 3-4**.** (**A**) Representative macroscopic poking-evoked current traces from cells expressing unmodified 86 and 1591 constructs (control), or the same constructs harboring mutations L2475I-V2476I (LI-VI) or M2241R-R2482H (MR-RH). Cells were stimulated using 3 µm poking stimuli for 500 ms at a holding potential of -80 mV or +80 mV. (**B-C**) The $Tau_{inactivation}$ values obtained by fitting the decaying current traces shown in (A) at +80 mV (B) and -80 mV for the indicated constructs. (**D**) Current density plots for data obtained in (B-C). (**E**) Representative fluorescence images and time course of cpGFP fluorescence traces from cells transfected with mutated and control 86 (top) and 1591 (bottom) constructs and acutely stimulated with a single 10 s / 0.28 Pa flow pulse. Scale bars = 10 µm. (**F**) Scatter plots showing $m\Delta F/F_0$ values from experiments described in (E). Each dot in (B-D) and (F) represents data from independent experiments. Numbers above plots in (B-D) and (F) indicate p-values from Kruskal-Wallis tests with Dunn's multiple comparisons against control. Error bars = s.e.m.